Effect of impurities on the charge-density-wave dynamics in $Ta_{1-x}Nb_xS_3$ alloys

D. Reagor
Los Alamos National Laboratory, Los Alamos, New Mexico 87544

G. Grüner
Department of Physics and Solid State Science Center, University of California, Los Angeles, Los Angeles, California 90024

(Received 21 April 1988; revised manuscript received 12 September 1988)

We report conductivity and dielectric-constant measurements on a series of orthorhombic $Ta_{1-x}Nb_xS_3$ alloys, with nominal concentrations between 0% and 0.3%, in the dc to 100-GHz frequency range. The Peierls transition observed at $T_P=220$ K in the pure specimens is smeared and suppressed in the alloys. The pinned–charge-density-wave mode, which occurs at the pinning frequency of $\omega_0/2\pi\sim 5$ GHz in the nominally pure specimen, increases with increasing dopant concentration at all temperatures. We analyzed the pinned mode in terms of a harmonic-oscillator response and found that the effective mass m^* and damping constant $1/\tau$ are independent of the impurity concentration. We also discuss the temperature dependence of ω_0 and τ and compare with the available theoretical descriptions of charge-density-wave dynamics.

I. INTRODUCTION

The pinning of the electron-hole condensate called the charge-density wave (CDW) by lattice imperfections, by grain boundaries, and by finite-size effects has been studied in detail in various compounds.[1] Pinning leads to a shift of the collective-mode oscillator strength to finite frequencies, with a so-called pinning frequency ω_0 that is generally well below the frequency corresponding to the single-particle gap $2\Delta/\hbar$. Extensive experiments performed in the dc–to–millimeter-wave spectral range[2] have been analyzed assuming that the collective response is described by the equation of motion,[3,4]

$$\frac{d^2\phi}{dt^2}+\frac{1}{\tau}\frac{d\phi}{dt}+\omega_0^2\phi=\frac{e}{m^*\lambda}E\ , \tag{1}$$

where τ is the relaxation time, m^* is the effective mass of the condensate, λ is the CDW wavelength divided by 2π, and ϕ is the phase of the CDW. Deviations from Eq. (1) have been observed[5,6] for $\omega<\omega_0$ and have been interpreted in terms of a tunneling model[7] and alternatively by assuming that disorder caused by randomly distributed impurities plays an important role and leads to a distribution of pinning frequencies.[5] Models[8–10] that include the internal degrees of freedom of the condensate also provide a semiquantitative account of the experimental findings. The above approaches lead to qualitative agreement with both the real and imaginary parts of the frequency-dependent conductivity, $\mathrm{Re}\sigma(\omega)$ and $\mathrm{Im}\sigma(\omega)$, over a large frequency range in the materials $NbSe_3$, orthorhombic TaS_3 (called TaS_3 in the following), $(TaSe_4)_2I$,[11] and $(NbSe_4)_2I$.[12]

In recent publications low-frequency data obtained in $NbSe_3$ and TaS_3 and estimations of other parameters involved were used to argue that the tunneling model describes $\sigma(\omega)$ over the full spectral range,[7] and similar conclusions[8,9] were reached on the basis of classical dynamics of the so-called Fukuyama-Lee-Rice model.[13] The conclusions were largely based on estimated values of the effective mass and on comparisons between the parameters obtained for the different model compounds $NbSe_3$ and TaS_3. Experiments that directly determine the dynamical parameters involved, preferably on a series of materials where some of the parameters are the same, may lead to more direct information than that quoted above. Aside from the question of the quantum versus classical approach to CDW dynamics, several other important features of CDW dynamics are unresolved, such as the nature of the damping and its dependence on impurity concentration, the detailed dependence of the pinning energy on the strength of the impurities, and the effect of temperature on the dynamics.

In this paper we report our measurements of $\sigma(\omega)$ in the microwave and millimeter-wave regime in $Ta_{1-x}Nb_xS_3$ alloys and also compare our observations with those made earlier on the ω- and E-dependent response. In contrast to $NbSe_3$, orthorhombic TaS_3 undergoes a metal-to-insulator transition at $T=220$ K (for the nominally pure material), indicating that the whole Fermi surface is removed by the formation of CDW's. Also, only one type of chain exists in the material,[1] making it a conceptually more straightforward example of CDW transport. The experimental results leads us to conclude that a temperatures not far below the Peierls transition the main features of $\sigma(\omega)$ observed in the millimeter-wave range may be adequately described with a simple harmonic-oscillator response. The effective mass m^* is within the experimental error, independent of the impurities. The pinning frequency ω_0 increases sharply with increasing x, but the relaxation time τ is independent of the impurity concentration. It is clear, however, that the simple approach based on Eq. (1) is not adequate at low temperatures where the fits differ significantly from the experimental results. The low-frequency dielectric constant ϵ decreases with increasing x and the

threshold field for the onset of nonlinear conduction, E_T, increases with increasing x, with a concentration dependence compatible with simple descriptions of CDW dynamics; however, the magnitude of both quantities is very different from those that are derived on the basis of simple models by using the pinning frequency ω_0 as an input parameter.

In Sec. II we describe the experimental details. This is followed in Sec. III by the summary of experimental results. We then present the analysis of $\sigma(\omega)$ in Sec. IV, discuss the parameters in detail, and make a comparison with the low-frequency ac- and nonlinear dc-conductivity results. Section V contains our conclusions. Some of the results we present in this paper have been reported earlier.[14–17]

II. EXPERIMENTAL TECHNIQUES

We prepared TaS_3 and $Ta_{1-x}Nb_xS_3$ alloys by direct reaction of the elements in sealed tubes. Gradient furnaces with a relatively weak temperature gradient centered around $T=535\,^{\circ}C$ were used. We obtained relatively large single crystals (typically 1 cm$\times$10 μm$\times$30 μm) within a period of a few days. Powder x-ray diffraction performed on the majority of alloys confirmed the phase to be orthorhombic.[15] Attempts to use analytical methods to evaluate the impurity concentrations were not successful; therefore the concentrations referred to in this paper are nominal. Because of this ambiguity, we could not evaluate the precise concentration dependence of the parameters that characterize the ω- and E-dependent response. Nevertheless, as will be demonstrated below, useful information can be obtained on the dynamics of the collective mode without detailed knowledge of the actual impurity content of the specimens.

We measured the dc resistivity with a conventional four-probe method, and evaluated the electric-field-dependent conductivity with short pulses to avoid heating effects. Standard cryogenic techniques were used to cool the specimens and to measure and regulate the temperature.

The samples prepared by the gradient-furnace technique are long, thin single crystals, with the long axis corresponding to the $\hat{\mathbf{b}}$ crystalographic axis. The $\hat{\mathbf{b}}$ axis is the high-conductivity axis of this quasi-one-dimensional metal and is always aligned with the electric field in these measurements. The conductivity along that axis determines the skin depth in the material and is the only component of the conductivity tensor measured. At room temperature the $\hat{\mathbf{b}}$-axis conductivity is 2500 $(\Omega\,\mathrm{cm})^{-1}$, implying a skin depth at 10 GHz of approximately 5 μm. The transverse dimensions of the crystals, as grown, were usually larger than 5 μm, and the pure specimens, where $\sigma(\omega)$ is large even at low temperatures, were cleaved along the long axis with the most desirable cross section being a few square micrometers. At the larger impurity concentrations, however, the microwave conductivity has an activated temperature dependence and both $\mathrm{Re}\sigma(\omega)$ and $\mathrm{Im}\sigma(\omega)$ are lower than in pure specimens. Consequently, to obtain adequate sensitivity at low temperatures, samples up to 10 μm in diameter were chosen.

The apparatus for the resonant-cavity measurements (4.5 and 9 GHz) is identical to that discussed earlier.[18] The cavities were coupled to a microwave network which measured the Q (quality factor) and resonant frequency of a mode of the cavity. The resonance may be measured in either the transmission or reflection mode. The fraction of the power reflected or transmitted near resonance is given by

$$\frac{P}{P_i}=A+B\left|\frac{i\omega}{(\omega_0')^2-\omega^2+i\omega\Gamma}\right|^2, \tag{2}$$

where $A=0$ and B is positive in transmission, and A is large and B is negative in reflection. The resonant frequency $\omega_0=\omega_0'+i\Gamma/2$ is generally complex, and Eq. (2) may be rewritten as

$$P=P_i\left[A+B\frac{1}{(\omega-\omega_0')^2+(\Gamma/2)^2}\right]. \tag{3}$$

The reflected or transmitted power has the Lorentzian form above when the frequency of the incident power, ω, is swept through the resonant frequency. The resonance paramenters ω_0' and Γ are the center frequency and full-width at half-height, respectively.

We recorded the cavity resonance with and without the sample and used the change in the resonance to calculate the complex conductivity, or equivalently, the complex dielectric constant. For the 9-GHz measurements we placed the samples on a Teflon platform and rotated them in and out of the microwave cavity with a set of gears and a control rod extending from room temperature to the cryogenic environment. At 4.5 GHz we placed the samples in a quartz tube and moved them in and out of the cavity with a sliding control rod that also extended to room temperature. By moving the samples in and out of the cavity, we measured all of the quantities needed to calculate the dielectric constant in a single cooling. The cavity was mounted at the bottom of a probe extending into a liquid-He^4 Dewar. Temperatures below 2 K could be obtained by pumping on the He^4 bath.

The response of the sample may be written in terms of complex conductivity ($\sigma=J/E$) or a complex dielectric constant ($\epsilon=D/E$). These are related via Maxwell's equations by $\epsilon=1+4\pi\sigma/i\omega$, where $i=\sqrt{-1}$ and ω is the angular frequency. In the limit of samples with a transverse dimension smaller than or comparable to the skin depth, the electric field inside the sample is given by

$$E=\frac{E_0}{1+N(\epsilon-1)}, \tag{4}$$

where E_0 is the field without a sample, ϵ is the dielectric constant normalized to the dielectric constant of free space, and N is the depolarization factor. The depolarization factor is a purely geometric quantity and, if the sample is approximated as an ellipsoid of transverse dimensions a,b and length L (with $L\gg a,b$), then[19]

$$N=\frac{ab}{L^2}\left[\ln\left[\frac{4L}{a+b}\right]-1\right]. \tag{5}$$

N reflects the ability of charges to build up at the ends of the sample and screen the applied electric field. For extremely long and slender samples, $N \sim 0$, and therefore $E \sim E_0$, the continuity condition for electric fields tangential to a surface is reproduced. This approach assumes that the electric field is uniform over the region in which the sample is placed, a condition that is easily achieved for samples much smaller than the cavity.

The samples used in this study were always much smaller than the resonant cavity, and the changes in the resonant frequency caused by the sample were only 1 MHz or less. The small changes in resonant frequency could be described by the resonant-cavity perturbation theory of Bethe and Schwinger,[20] which relates the change in electric field to the change in resonant frequency. Using Eq. (4) the resonant-frequency shift [$\delta\omega_0 = \omega_0$(sample in) $-\omega_0$(sample out)] is[21]

$$\frac{\delta\omega_0}{\omega_0'} = \frac{-\alpha(\epsilon-1)}{1+N(\epsilon-1)} , \tag{6}$$

where α is the filling factor—$\alpha = 2.1(V_s/V_c)$, where V_s and V_c are the volume of the sample and cavity, respectively—and $\delta\omega_0 = \delta\omega_0' + i\,\delta\Gamma$ is complex for material with a loss term in the dielectric constant. Experimentally, $\delta\omega_0'$ is the shift in resonant frequency and $\delta\Gamma$ is the change in the half-width of the resonance at half-height. The formula may be inverted[21] to solve for ϵ and separated into real and imaginary parts to yield the full complex dielectric constant:

$$\mathrm{Re}(\epsilon) = 1 + \frac{1}{N}\frac{\delta\omega_0'(\alpha/N - \delta\omega_0') - (\delta\Gamma)^2}{(\delta\Gamma)^2 + (\alpha/N - \delta\omega_0')^2} , \tag{7a}$$

$$\mathrm{Im}(\epsilon) = \frac{\alpha}{N^2}\frac{\delta\Gamma}{(\delta\Gamma)^2 + (\alpha/N - \delta\omega_0')^2} . \tag{7b}$$

The two constants in the analysis, α and N, may be determined from the geometry of the sample. [See Eq. (5) and the discussion following Eq. (6).] In practice, however, a precise measurement of the sample dimensions and the approximation of the actual crystal geometry as an ellipsoidal cylinder lead to errors of up to 50% in the calculated values of α and N. More precise values are obtained by taking the room-temperature value of $\delta\omega/\omega_0$ (well above the phase transition) and choosing α and N such that the real part of the conductivity is equal to the dc conductivity at room temperature and the imaginary part of the conductivity is zero. This procedure assumes that the sample behaves as a normal metal well above the Peierls transition. One should note, however, that fluctuation effects caused by the quasi-one-dimensional structure of the compound are important above T_p and lead to a pseudogap and, consequently, to the possibility of frequency-dependent response even at millimeter-wave frequencies. These effects are most probably an important factor at temperatures not much above the Peierls transition temperature where the temperature dependence of the dc resistivity is distinctively nonmetallic. At room temperature, however, the temperature dependence of the dc resistivity is that of a metal. Consequently, we assume that $\sigma(\omega)$ is that of a metal at room temperature [i.e., $\mathrm{Re}\sigma(\omega)$ is independent of the frequency]. With this assumption all the variables in Eq. (6) are determined and the complex dielectric constant may be determined from the measured values of $\delta\omega_0'$ and $\delta\Gamma$.

We performed the millimeter-wave conductivity measurements (30, 32, 60, 94, and 109 GHz) with a millimeter-wave bridge technique discussed in earlier publications.[18,22] The technique involves placing samples in a section of shorted waveguide and using the change in impedance of the waveguide to calculate the conductivity of the sample. The samples are cleaved to a diameter of a few micrometers, similar to the cavity measurements. We attach the small samples electrostatically to a quartz fiber and insert the quartz and sample through a small hole in the top of the waveguide, with the electric field parallel to the long axis of the sample. The hole is at an antinode of the electric field a distance $3\lambda/4$ (where λ is the guided wavelength) from the waveguide-shorting plate. The shorted-waveguide section is on the sample arm of a millimeter-wave impedance bridge. The design and operation of the bridge are extensively discussed in Ref. 22. The bridge consists of passive components as well as precision attenuators and phase shifters on sample and reference arms. When the attenuation and phase shifters are adjusted properly, the waves traveling the two arms are 180° out of phase and equal in amplitude, resulting in a null at the detector.

The components of the millimeter-wave bridge are separated from the sample holder by an 8-in. section of stainless-steel waveguide. A helium-gas-flow system placed around the sample-arm waveguide cools the sample holder down to 20 K. The application of a smooth gas flow causes highly reproducible phase-shift and attenuation readings because of thermal effects originating in the apparatus, such as thermal contraction of the waveguide, in addition to sample effects. We perform two coolings, one with sample in and one with sample out, and record the attenuation and phase readings on each run. The absolute values contain systematic artifacts, but the differences in attenuation and phase are determined by the sample.

The introduction of the specimen leads to changes in the amplitude and phase of the transmitted signal, which we interpret as follows. If we define the change in the complex phase as $\delta\Phi = \delta\phi + i\,\delta x\,[\ln(10)/20]$, where δx is the change in attentation (in units of dB) and $\delta\phi$ is the change in phase, then, from standard microwave theory,

$$\tan\left[\frac{-\Delta\Phi}{2}\right] = \frac{(iY_{\mathrm{in}} - iY_{\mathrm{out}})/Y_0}{1 + iY_{\mathrm{in}}iY_{\mathrm{out}}/Y_0^2} , \tag{8}$$

where Y_{in} and Y_{out} are the admittances with and without the sample (sample in and sample out), respectively. The form above is invariant to transformations down the transmission line and may be evaluated at any position. For simplicity, we chose to evaluate the admittances at the sample position. The short must be transformed by a

distance $-3\lambda/4$ (defining the positive direction towards the shorting plate) and becomes an open circuit ($Y_{\text{out}}=0$). Determining Y_{in} is generally a complicated calculation, but for a sample approximated as a right circular cylinder of radius R traversing the waveguide with the long axis parallel to the electric field the admittance has been calculated by Schwinger and Saxon[23] and is given in the small-sample limit by

$$\left[\frac{Y_s}{Y_0}\right]^{-1}=i\frac{a}{2\lambda_g}\left[\ln\left[\frac{2a}{\pi R}\right]-2+2\sum_{\text{odd } n\geq 3}\left[\frac{1}{[n^2-(2a/\lambda)^2]^{1/2}}-\frac{1}{n}\right]\right]-i\frac{a}{\lambda_g}\frac{1}{(kR)^2(\epsilon-1)}\ , \tag{9}$$

where R is the radius of the sample, a is the transverse dimension of the waveguide, λ is the wavelength in free space, λ_g is the guided wavelength, k is the free-space wave vector, and ϵ is the complex dielectric constant. The small-sample limit assumes that the sample radius is smaller than a skin depth. The general form in Ref. 23 implies that deviations from Eq. (9) are small for several skin depths. The first term, denoted Y_0/Y_∞, is independent of the dielectric constant, and for large ϵ it is the only term remaining. The geometry assumed in Ref. 23 places the sample in perfect electrical contact to the interior surface of the waveguide. This geometry is not possible in practice, and the sample did not normally make electrical contact to the waveguide. The small gap at the ends of the sample may be represented as a capacitance in series with the sample.[18,22] The equivalent circuit is therefore given by

$$\frac{1}{Y_{\text{in}}}=\frac{1}{Y_s}+\frac{1}{Y_c}=\frac{1}{Y_\infty}+\frac{1}{Y_c}-i\frac{a}{\lambda_g}\frac{Y_0^{-1}}{(kR)^2(\epsilon-1)}\ . \tag{10}$$

The dielectric constant derived from Eqs. (8)–(10) is therefore

$$\epsilon=1+\frac{a}{\lambda_g(kR)^2}\left[\frac{1}{\tan(\Delta\Phi/2)}-\frac{iY_0}{Y_c}-\frac{iY_0}{Y_\infty}\right]^{-1}\ , \tag{11}$$

and may be separated into real and imaginary parts:

$$\text{Re}(\epsilon)=1+\frac{a}{\lambda_g(kR)^2}\frac{\text{Re}[\cot(\Delta\Phi/2)]-i(Y_0/Y_\infty+Y_0/Y_c)}{\{i(Y_0/Y_c+Y_0/Y_\infty)-\text{Re}[\cot(\Delta\Phi/2)]\}^2+\text{Im}[\cot(\Delta\Phi/2)]^2}\ , \tag{12a}$$

$$\text{Im}(\epsilon)=\frac{-a}{\lambda_g(kR)^2}\frac{\text{Im}[\cot(\Delta\Phi/2)]}{\{i(Y_0/Y_c+Y_0/Y_\infty)-\text{Re}[\cot(\Delta\Phi/2)]\}^2+\text{Im}[\cot(\Delta\Phi/2)]^2}\ . \tag{12b}$$

As with the cavity method, the analysis requires two parameters—$Y_0/Y_c+Y_0/Y_\infty$ and $a/\lambda_g(kR)^2$. We determined these parameters by setting $\text{Re}(\sigma)=\sigma_{\text{dc}}$ and $\text{Im}(\sigma)=0$ at room temperature and solving for the parameters, which we then assumed to be independent of temperature (although thermal contraction leads to an error of $\approx 1\%$).

The complex-dielectric-constant measurements presented in the following section use the two methods discussed above: the bridge technique at 30, 60, 94, and 109 GHz and the cavity technique at 4.5 and 9 GHz.

III. RESULTS

Figure 1 displays the temperature dependencies of the low-field dc conductivities of pure TaS_3 and $Ta_{1-x}Nb_xS_3$. The phase transition at 220 K is not evident from the direct $\sigma_{\text{dc}}(T)$ plots, but the derivative $d\sigma/dT$ or dR/dT has a sharp cusp at the Peierls transition. Because of the logarithmic plot, data taken on the alloys were indistinguishable from data taken on the pure samples, and measurements on several crystals indicate that the magnitude of the dc conductivity is, within the experimental error of approximately 10%, also independent of the concentration. This result is expected because a small amount of impurities (less than 1%) in a metal is not expected to lead to a resistivity comparable to the phonon $T=300$ K resistivity. The temperature derivative of the resistivity clearly shows the effect of impurities on the phase transition. Figure 2 shows $(-1/R)(dR/dT)$ for the pure specimens and for two alloys with $x=0.001$ and 0.002. The transition is progressively broadened by the introduction of impurities, and the peak in the temperature derivative moves to lower temperatures. Figure 3 shows the concentration dependence of T_p, where T_p is defined as the peak in $(-1/R)(dR/dT)$, versus the nominal concentration. We observe a linear depression of T_p, with

$$\frac{dT_p}{dx}=70\ \text{K/at. \%}\ . \tag{13}$$

We stress again, however, that x refers to nominal concentration that may differ from the actual impurity concentration in the specimens we have investigated. Recent experiments on irradiated specimens[24] did not display a linear decrease and were in agreement with a square-law behavior, $\Delta T_p \propto -x^{1/2}$, in clear contrast with Eq. (13). Whether this represents a real difference between the effects of substitutional impurities and radiation defects or is due to the poorly defined x values in Fig. 3 remains to be seen. The main conclusions of our paper, however, do not rely on the precise values of x.

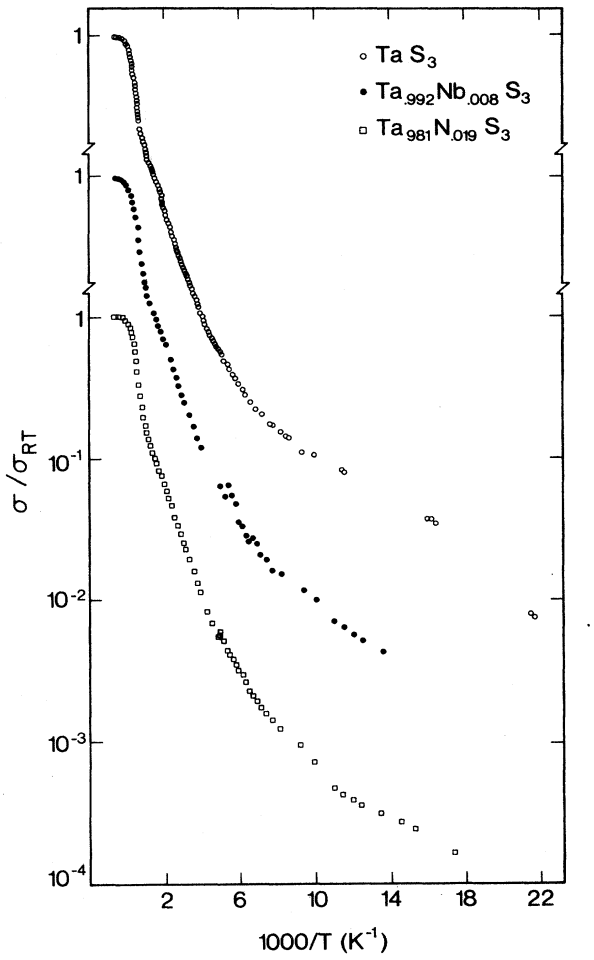

FIG. 1. Temperature dependence of the dc conductivity of nominally pure orthorhombic TaS_3. σ_{RT} refers to the room-temperature dc conductivity. The average value, $\sigma_{RT}=2500$ $(\Omega\,\mathrm{cm})^{-1}$, was determined from measurements made on several single crystals.

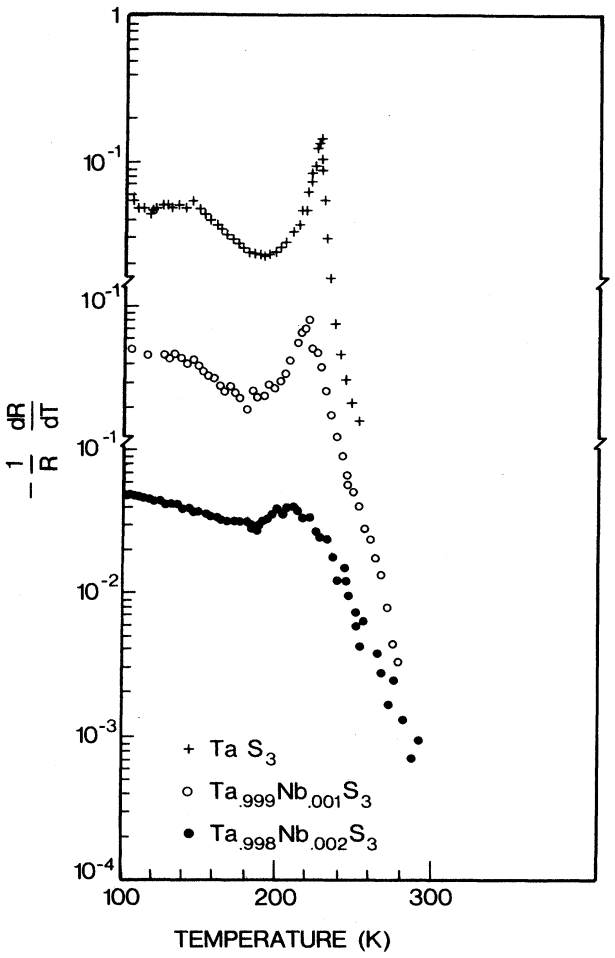

FIG. 2. Temperature dependence of the derivative $(-1/R)(dR/dT)$ in nominally pure TaS_3 and in $Ta_{1-x}Nb_xS_3$ alloys.

Figure 4 displays the response at millimeter-wave frequencies in nominally pure TaS_3. We presented and extensively discussed these results in a previous publication[16] and here we only shortly summarize the main experimental findings. The response, when analyzed in terms of Eq. (1), is overdamped, i.e., $\omega_0\tau \ll 1$. Equation (1) is a simple harmonic-oscillator response; hence the quality factor is $Q=\omega_0\tau$. In the regime above 100 K but well below the transition temperature, the resonant frequency, $\omega_0/2\pi$, is approximately 5 GHz and the resonance width, $1/2\pi\tau$, is approximately 100 GHz, implying $Q \ll 1$. The temperature dependence of these parameters is weak, changing by 20–30% over the entire high-temperature range (i.e., between 100 K and T_p). Below 100 K the temperature dependence of the measured conductivities is much stronger than that found at high temperatures. The 9-GHz conductivity rises immediately below 100 K, but begins a rapid decrease near 80 K. The 30- and 60-GHz conductivities also increase slightly, then decrease as the temperature is decreased. The dielectric constants become less negative, eventually crossing zero at temperatures well below 100 K. For the response implied by Eq. (1), the dielectric constant is positive below ω_0 and negative above ω_0. The conductivity [Re(σ)] also reaches a maximum at ω_0. If we qualitatively express the temperature dependence of σ in terms of ω_0 and $1/\tau$, then ω_0 remains approximately 5 GHz above 100 K, but increases sharply at lower temperatures. The damping, $1/\tau$, remains weakly temperature dependent over the entire temperature range of the measurements. In general, the spectral weight remains at low frequencies above $\simeq$100 K with a clear movement to higher frequencies below 100 K. Also, although we found the simple harmonic oscillator appropriate at temperatures above 100 K, at low temperatures the agreement between Eq. (1) and the experimental results becomes poor, and a description in terms of the single-particle model is not possible (see below).

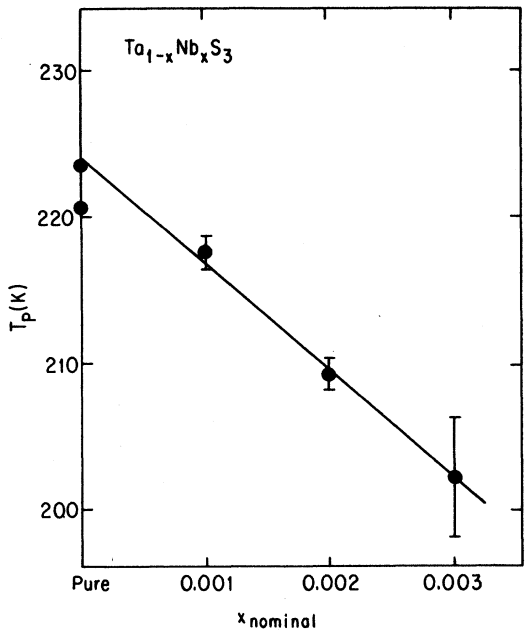

FIG. 3. Concentration dependence of the transition temperature T_p in $Ta_{1-x}Nb_xS_3$ alloys. The solid line leads to $dT_p/dc = 70$ K/at. %.

We believe that the reason for the peculiar (i.e., nonmonotonic) temperature dependencies observed in both $\mathrm{Re}\sigma(\omega)$ and $\mathrm{Im}\sigma(\omega)$ is the commensurate-incommensurate transition that occurs around 100 K. This transition, evident from some structural studies,[25] leads also to peculiar temperature dependencies of the nonlinear dc conduction. Because of this effect, the detailed temperature dependence of the dynamics of the collective mode is complicated, and we do not speculate on the effect of commensurability on the ac response of the pinned collective mode.

We present the temperature dependence of the conductivity and dielectric constant in Fig. 5 for $x=0.001$ and in Fig. 6 for $x=0.002$. Contrasting the measured values of $\mathrm{Re}\sigma(\omega)$ and $\mathrm{Re}\epsilon(\omega)$ shows that the conductivities and dielectric constants change by orders of magnitude with increasing impurity concentration. This change is due to a general shift of spectral weight of the collective CDW response to higher frequencies with increasing impurity concentration. The figures also show that in the temperature range between 100 and 200 K the frequency where the maximum conductivity occurs, $\omega_0/2\pi$ in terms of Eq. (1), is increasing from approximately 5 GHz for the nominally pure samples to nearly 100 GHz for the samples with $x=0.002$. Figure 7 presents the results for $Ta_{0.997}Nb_{0.003}S_3$ samples from experiments performed only at one frequency, 94 GHz. The dielectric constant is positive and the conductivity is rapidly decreasing below the transition, indicating a pinning frequency significantly larger than 94 GHz.

IV. ANALYSIS

The experimental results presented above clearly show that a small amount of impurities has a profound effect on both the statics and dynamics of CDW's. We will first

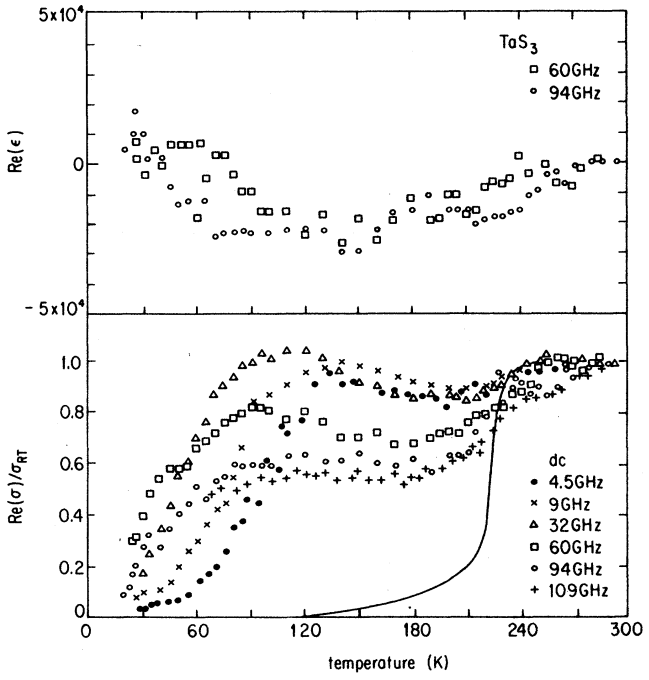

FIG. 4. Temperature dependence of the conductivity and dielectric constant in pure TaS_3 at various frequencies. The solid line is the dc conductivity.

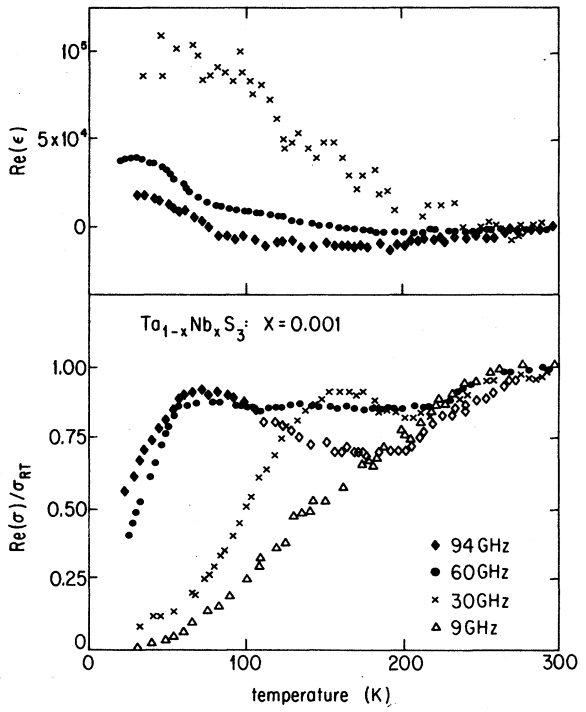

FIG. 5. Temperature dependence of the conductivity and dielectric constant in $Ta_{0.999}Nb_{0.001}S_3$, at various frequencies.

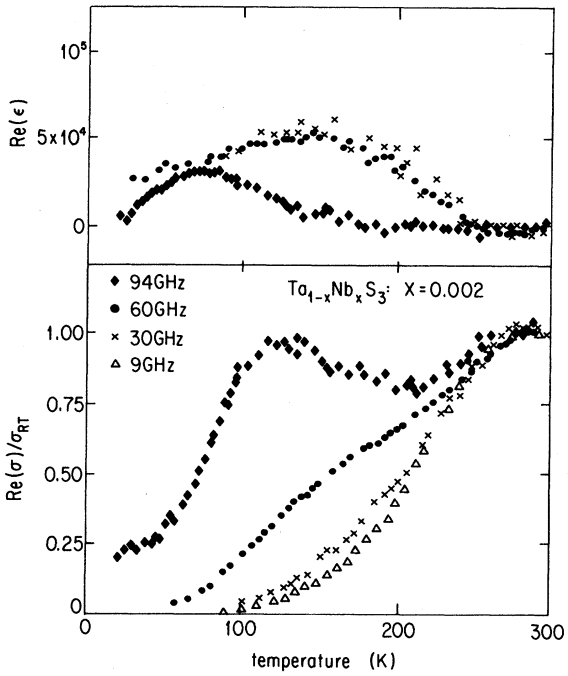

FIG. 6. Temperature dependence of the conductivity and dielectric constant in $Ta_{0.998}Nb_{0.002}S_3$, at various frequencies.

comment on the effects of impurities on the transition and then discuss in more detail the effect of impurities on the dynamics. The discussion of the dynamical effects will treat the microscopic origin of the parameters in Eq. (1), the details of fits to the experimental results, and the interpretation of deviations from Eq. (1). Lastly, we will

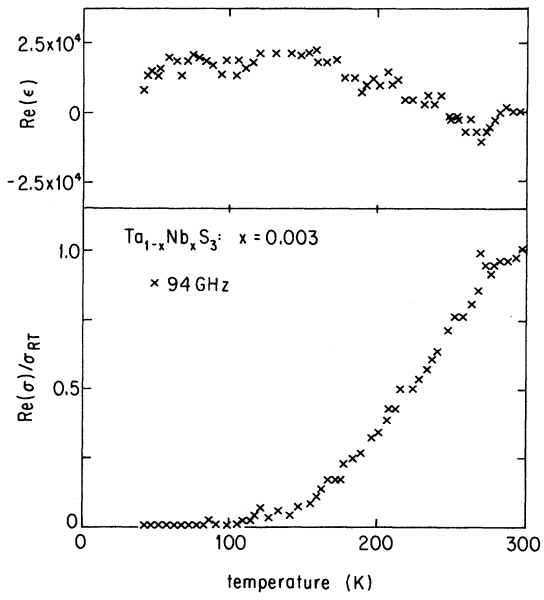

FIG. 7. Temperature dependence of the conductivity and dielectric constant in $Ta_{0.997}Nb_{0.003}S_3$, at 94 GHz.

compare the temperature and impurity dependence of ω_0 with the low-frequency quantities $\epsilon(\omega=0)$ and E_T.

The standard model that treats the interaction between impurities and CDW's has been proposed by Fukuyama,[13,26] Lee and Rice,[13] and by Efetov and Larkin.[27] The Hamiltonian is given by

$$H=\tfrac{1}{2}\kappa\int(\nabla\phi)^2 d\mathbf{r}+V_0\rho_1\sum_i\cos[2k_F r_i+\phi(r_i)]\ , \qquad (14)$$

where ϕ is the phase of the condensate, V_0 is the impurity potential, κ is the elastic constant associated with the CDW deformations, ρ_1 is the CDW amplitude, and i represents the impurity positions. The Hamiltonian, in the limit when $\nabla\phi$ is small, is equivalent to the random-field XY model.[28] The $(\nabla\phi)^2$ representing the phase excitations leads to a gapless mode, and Sham and Patton,[29] and Imry and Ma,[30] have shown that in less than four dimensions long-range order is absent. The effect of impurities in this case is dramatically different than, for example, that in superconductors or ferromagnets. In the latter cases, the transition remains sharp (mean-field-like) and only T_c is depressed by impurities. In contrast, we observe a dramatic broadening of the transition in CDW's. Other observers have seen similar effects in irradiated specimens.[24]

We are not aware of a detailed theory that treats the impurity-induced smearing of the phase transition, but we expect that impurities lead to an upper limit of the phase-phase coherence length and that this cutoff leads in turn to a smearing of the phase transition. Further studies are required to clarify this point.

The CDW, as described by Eq. (14), is capable of nonlinear conduction in the presence of a large electric field. This nonlinearity, the so-called Fröhlich mode, is well documented experimentally and is the subject of extensive studies.[1] Within the model, Eq. (14), we may derive expressions for the threshold field for sliding, E_T, and ω_0, the pinning frequency in Eq. (1). In addition, we may calculate the low-frequency dielectric constant $\epsilon(\omega=0)$ in terms of ω_0. Fits to determine ω_o and comparisons with E_T and $\epsilon(\omega=0)$ will then determine the suitability of the description and approximate values of the parameters in Eq. (14).

The first term in Eq. (14) favors a spatially homogenous phase, whereas the second term favors local distortions of the phase of the CDW to minimize the energy at the impurity sites. Within this one-dimensional theory the ratio

$$\alpha=\frac{V_0\rho_1}{\hbar V_F n_i} \qquad (15)$$

tells whether the potential energy or elastic energy is more important; $\alpha>1$ is called strong impurity pinning and $\alpha<1$ is weak impurity pinning.

In each limit the pinning frequency ω_0 may be calculated; however, the relations between ω_0, ϵ, and E_T do not depend on which limit is appropriate. The energy necessary to overcome the pinning potential is approximately the energy necessary to displace the phase at the CDW by a quarter-wavelength in the harmonic potential.

Therefore, $eE_T\lambda/4=\frac{1}{2}m^*\omega_0^2(\lambda/4)^2$, or

$$E_T=\frac{m^*\omega_0^2\lambda}{8e} . \tag{16}$$

Also, the dielectric constant at low frequencies, $\epsilon(\omega=0)$, depends only on the spectral weight ne^2/m^* and the pinning frequency ω_0,

$$\epsilon(\omega=0)=\beta\frac{4\pi ne^2}{m^*\omega_0^2} , \tag{17}$$

where the constant β is 1 for a harmonic oscillator and of order unity for a mode centered at ω_0. In the above equations we have neglected the infinite-frequency dielectric constant.

The static microscopic model in Eq. (14) may be extended to dynamical problems by adding a kinetic-energy term and deriving an equation of motion. The impurities and inertia alone produce a pinned mode with a finite linewidth. In addition to the disorder-induced linewidth, we add an intrinsic damping term to obtain the full linewidth of the mode. (We will show that this is a necessity.) Others have obtained approximate solutions of this model that will be discussed below, but we will first discuss the results in terms of Eq. (1), and use the microscopic models to interpret the parameters of the fits and the deviations from the fits.

(i) Strong pinning ($\alpha\gg1$). The CDW is pinned at the impurities and responds to the electric field with long-wavelength distortions in the region between impurities. The pinning frequency is approximately[13]

$$\omega_0=\left[\frac{m}{m^*}\right]^{1/2}V_Fn_i , \tag{18}$$

where n_i is the impurity density and $(m/m^*)^{1/2}V_F$ is the phase velocity (the so-called phason velocity).

(ii) Weak pinning ($\alpha\ll1$). In this limit[13] the resonant frequency is

$$\omega_0=\left[\frac{3}{\pi^2}\right]^{-2/3}\left[\frac{m}{m^*}\right]^{1/2}V_FL_0^{-1} , \tag{19}$$

where L_0 is the size of a phase-coherent domain given within the model by

$$L_0^{-1}=\left[\frac{3}{\pi}\alpha\right]^{2/3}n_i . \tag{20}$$

Clearly, $L_0^{-1}\ll n_i$, which results from the elastic energy preventing the phase from adjusting to each impurity potential. The impurity potentials within a domain then add randomly, leading to partial cancellation and a pinning energy lower than that expected from strong pinning. As α increases, L_0^{-1} approaches n_i and Eq. (19) is equal to Eq. (18) to within factors of order unity.

In contrast to the detailed theory of pinning, which suggest that in both limits ω_0 increases with increasing impurity concentration, little is known about the damping that accompanies the CDW motion. Although Fröhlich originally suggested that there is no damping, various interactions clearly can lead to the damping of the collective mode. The theories of the damping (linewidth) may be divided into two classes.

(1) Impurity scattering. The scattering of the CDW from impurities will pin the CDW, as discussed above, and will result in damping of the CDW. Estimates of the linewidth contribution[13] using the impurity model [Eq. (14)] imply $1/\tau\simeq\omega_0$ in both the strong- and weak-pinning limits. Any changes in ω_0 would be directly reflected in $1/\tau$, maintaining a constant product $\omega_0\tau\simeq1$.

(2) Intrinsic processes. The scattering of the CDW by other phasons has been treated by Takada, Wong, and Holstein.[31] The expressions they derive were discussed in an earlier publication.[2] The result of the theory at temperatures greater than or comparable to the Debye temperature is

$$\frac{1}{2\pi\tau}=\frac{\pi^3}{64(2)^{1/2}}\left[\frac{\lambda^2}{\mu\Omega_t}\right]T^2 , \tag{21}$$

where λ is the electron-phonon–coupling constant, $\mu=m^*/m_b$, with m_b the band mass, and ω_t is the transverse-phonon frequency. Previous estimates of $1/2\pi\tau$ at 150 K yielded 4 GHz, a value far lower than the experimental results in pure samples.

The last parameter in Eq. (1) is the effective mass of the CDW condensate. The effective mass follows from a microscopic theory[32] and is given by

$$\frac{m^*}{m_b}=1+\frac{4\Delta^2}{\lambda\omega(2k_F)^2} , \tag{22}$$

where Δ is the single-particle gap, λ is the dimensionless electron- phonon–coupling constant, and $\omega(2k_F)$ is the phonon frequency at wave vector $2k_F$ before the inclusion of electron-phonon interactions. With $\Delta\sim700$ K, $\lambda\sim\frac{1}{3}$, and $\omega(2k_F)=100$ K (parameters appropriate for TaS_3), $m^*/m_0\sim600$. This result is in rough agreement with the results for nominally pure TaS_3, where $m^*/m_e=1000\pm200$ over a wide range of temperatures.[2]

In addition to the CDW response, the experimental results contain conductivity contributions from the quasiparticles or "normal" electrons. This contribution is the dc conductivity σ_{dc} measured at low fields ($E<E_T$), where the CDW is pinned and will not contribute to the dc conductivity. For the following analyses of the frequency dependence, we subtract σ_{dc} from $\sigma(\omega)$ and call the difference in conductivity the CDW response.

The three fundamental parameters, with a single-degree-of-freedom description, are the pinning frequency, the damping constant, and the effective mass. Subsequently, we will focus on the concentration and temperature dependence of these parameters. Using σ for the CDW conductivity determined from Eq. (1), we have

$$\mathrm{Re}(\sigma)=\frac{ne^2\tau}{m^*}\frac{\omega^2}{\tau^2(\omega^2-\omega_0^2)^2+\omega^2} , \tag{23a}$$

$$\mathrm{Im}(\sigma)=\frac{ne^2\tau}{m^*}\frac{\omega\tau(\omega_0^2-\omega^2)}{\tau^2(\omega^2-\omega_0^2)^2+\omega^2} , \tag{23b}$$

We will apply these equations to the experimental results

as a starting point for discussion.

Figure 8(a) shows the frequency-dependent conductivity of nominally pure TaS_3 at 160 K. The response is overdamped, and consequently a logarithmic frequency scale is necessary to present the data. The lower-frequency results—from Wu *et al.*[5]—are measured on the same batch of crystals used for our measurements. The solid curve is Eq. (23a) with fit parameters $\omega_0/2\pi=5$ GHz and $(2\pi\tau)^{-1}=125$ GHz. We note that although agreement between the experiment and Eq. (23a) is adequate in the microwave and millimeter-wave spectral range, the agreement at low frequencies between the experimental results and Eq. (23a) is poor. The agreement may be corrected by including a distribution of pinning frequencies extending to low frequencies, but having a cutoff at higher frequencies. We will discuss these fits below.

Figure 8 shows that the CDW motion can be qualitatively described with a harmonic-oscillator response, and the fundamental parameters can be evaluated from such a fit. Disorder effects appear to modify the response only at frequencies below the pinning frequency ω_0, but do not influence the conclusion concerning the pinning and high-frequency damping of the collective mode. We are therefore proceeding by using Eq. (1) also for the analysis of the pinned collective mode in the doped specimens. Figures 9–13 display both $\mathrm{Re}\sigma(\omega)$ and $\mathrm{Im}\sigma(\omega)$ for the pure specimen and the alloys at different temperatures. At all temperatures we observe a sharp shift of the spec-

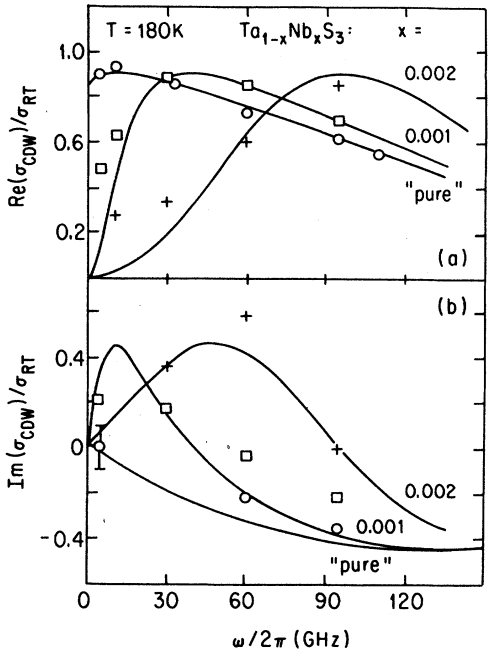

FIG. 9. Frequency dependence of $\mathrm{Re}\sigma(\omega)$ and $\mathrm{Im}\sigma(\omega)$ in $Ta_{1-x}Nb_xS_3$ alloys at $T=180$ K. The solid lines are fits to Eqs. (23a) and (23b) with parameters discussed in the text and also given in Figs. 14–16.

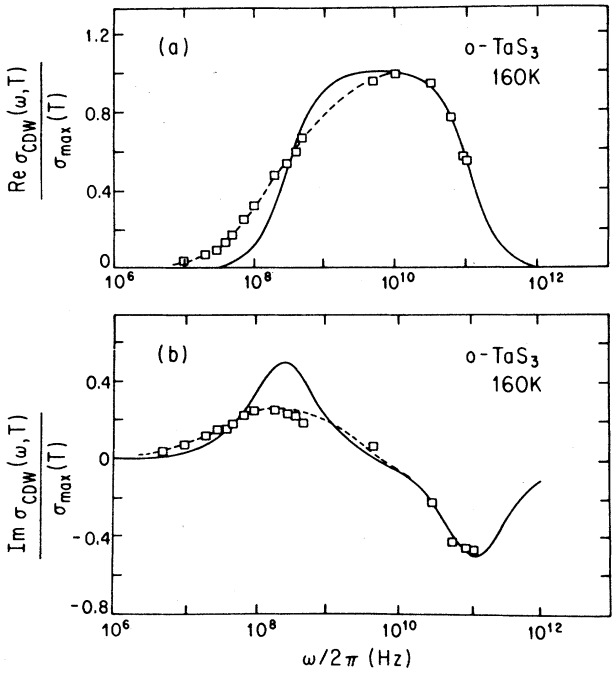

FIG. 8. Frequency dependence of $\mathrm{Re}\sigma(\omega)$ and $\mathrm{Im}\sigma(\omega)$ in nominally pure TaS_3 at $T=160$ K. The solid lines are fits to Eqs. (23a) and (23b) with parameters discussed in the text. The dotted line is a fit assuming a broad distribution of pinning frequencies; see Eq. (29) and Ref. 6.

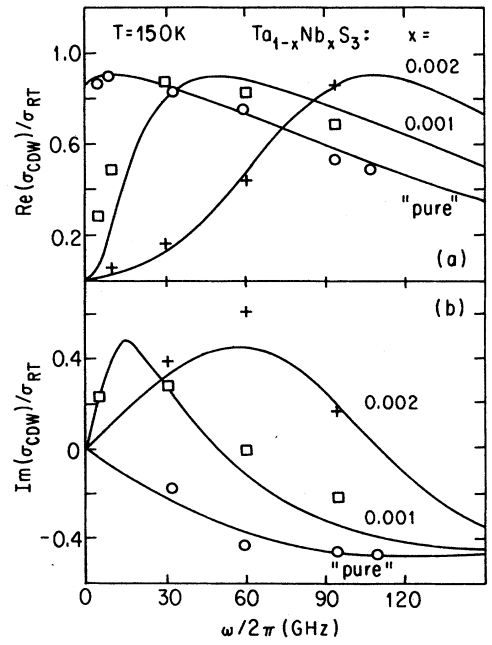

FIG. 10. Frequency dependence of $\mathrm{Re}\sigma(\omega)$ and $\mathrm{Im}\sigma(\omega)$ in $Ta_{1-x}Nb_xS_3$ alloys at $T=150$ K. The solid lines are fits to Eqs. (23a) and (23b) with parameters discussed in the text and also given in Figs. 14–16.

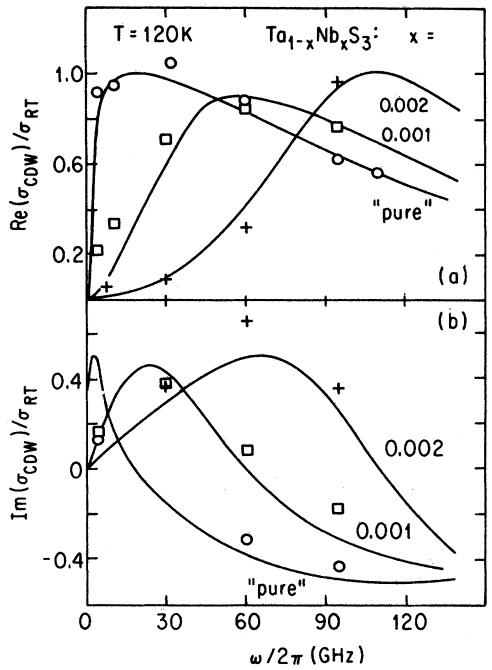

FIG. 11. Frequency dependence of $Re\sigma(\omega)$ and $Im\sigma(\omega)$ in $Ta_{1-x}Nb_xS_3$ alloys at $T=120$ K. The solid lines are fits to Eqs. (23a) and (23b) with parameters discussed in the text and also given in Figs. 14–16.

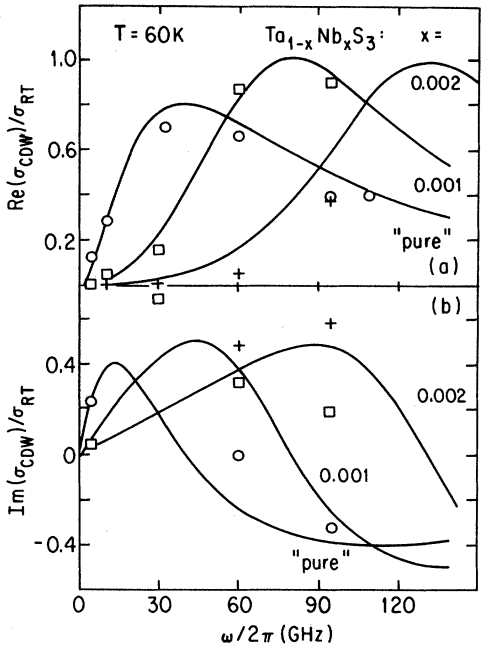

FIG. 13. Frequency dependence of $Re\sigma(\omega)$ and $Im\sigma(\omega)$ in $Ta_{1-x}Nb_xS_3$ alloys at $T=60$ K. The solid lines are fits to Eqs. (23a) and (23b) with parameters discussed in the text and given also in Figs. 14–16.

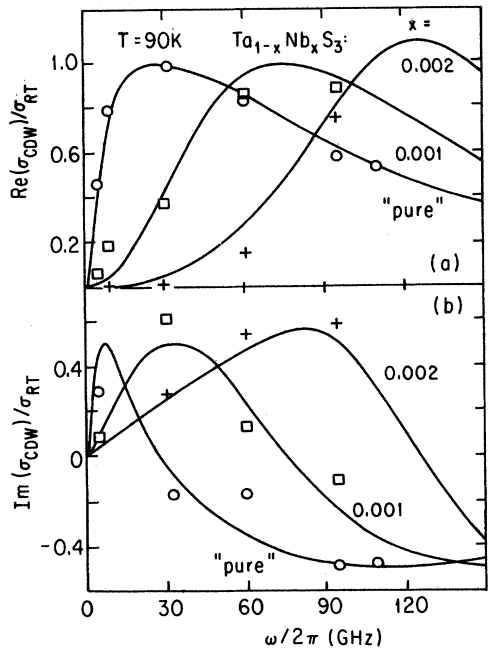

FIG. 12. Frequency dependence of $Re\sigma(\omega)$ and $Im\sigma(\omega)$ in $Ta_{1-x}Nb_xS_3$ alloys at $T=90$ K. The solid lines are fits to Eqs. (23a) and (23b) with parameters discussed in the text and also given in Figs. 14–16.

tral weight to higher frequencies with increasing impurity concentration. In addition, the maximum conductivity remains unchanged within experimental error. In the figures the solid curves are fits to Eqs. (23a) and (23b) for each impurity concentration.

We first note that a harmonic-oscillator response roughly accounts for both $Re\sigma(\omega)$ and $Im\sigma(\omega)$, especially at higher temperatures. The fit gets progressively less and less adequate at lower temperatures, and at 60 K only a gross overall agreement with the measured and calculated curves is recovered. We also note that for the higher-concentration alloys with $x=0.002$ and0.003 the fits are not accurately determined because only the lower spectral end of the resonance is within the spectral range of the measurements. Several facts, however, assist in evaluating $1/\tau$ and ω_0 in this case. The dc-conductivity studies demonstrate that the transition temperature is decreased by less than 10% for the most heavily doped samples ($x=0.003$). The single-particle gap is, within weak-coupling mean-field theory, linearly related to the transition temperature, implying that the doping produces an equally small change ($\simeq 10\%$) in the gap. Also, the dc-resistance curves for the materials are almost indistinguishable (see Fig. 1). That $\sigma(T)$ is determined by the gap below T_p also suggests that Δ is only weakly affected by the impurities. In the theories of the CDW excitation spectrum,[32] the effective mass is proportional to the square of the single-particle gap [see Eq. (22)], a result supported by our earlier work.[11] The change in effective mass, or equivalently the integrated spectral

weight, is therefore approximately 20%. This produces an additional constraint on the fit parameters, i.e. one expects that

$$\sigma_{\max}/\tau = ne^2/m^* = \text{const} , \tag{24}$$

where, in practice, the approximation as a constant is accurate to well within the 20% estimated above. The fits to Eqs. (23a) and (23b), with this additional constraint, are then accurately evaluated at the larger impurity concentrations.

Several conclusions can be drawn concerning the concentration dependence of the fundamental parameters of the problem, even without knowledge of the impurity concentration. First, the pinning is due to impurities and, except for the nominally pure specimens, pinning by grain boundaries, by contacts or by the surface of the specimens, does not play a significant role. Because of the absence of detailed information on the actual impurity concentration, we are not able to rigorously distinguish between the weak- and strong-impurity-pinning limits. We have performed an analysis, such as that presented before for the $T=150$ K data, at different temperatures, leading to the temperature dependence of the parameters $\omega_0/2\pi$ and $(2\pi\tau)^{-1}$ and $\sigma_{\max}/\sigma_{\mathrm{RT}}$ (RT denotes room temperature.) These results are displayed in Figs. 14 and 15 in the temperature range where the harmonic-oscillator fit provides an appropriate description of the experimental results.

In general, the pinning frequency increases with increasing impurity concentration at all temperatures, confirming the importance of impurity pinning TaS_3. Figure 16 plots the pinning frequency versus impurity concentration at selected temperatures. It appears, however, that the data cannot be simply described by the expression

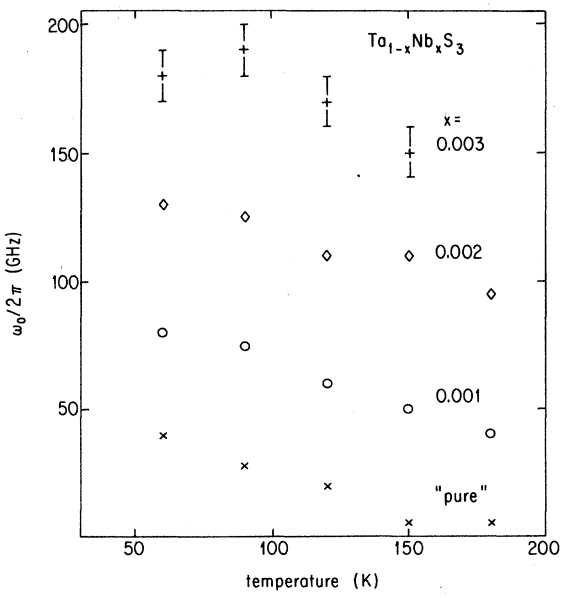

FIG. 14. Temperature dependence of the pinning frequency ω_0 in nominally pure and alloyed TaS_3 specimens.

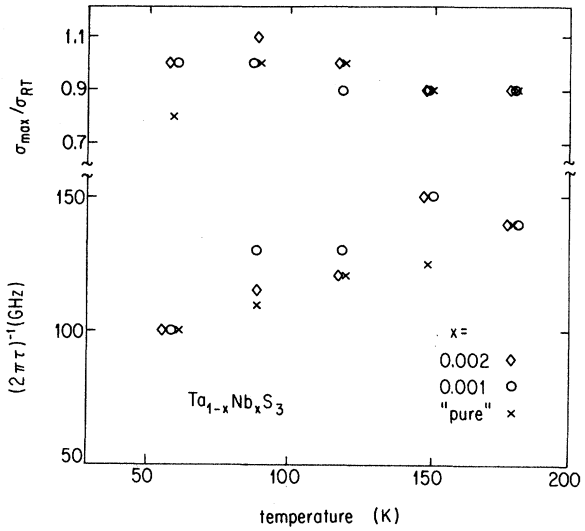

FIG. 15. Temperature dependence of the relaxation rate $(2\pi\tau)^{-1}$ and maximum conductivity $\mathrm{Re}\sigma(\omega=\omega_0)$ in nominally pure and alloyed TaS_3 specimens.

$$\omega_0 = A(T)f(x) , \tag{25}$$

with $f(x)\sim x^{\gamma}$ (with γ also depending on the impurity concentration), as would be required for a pinning frequency determined entirely by this type of impurity even for the nominally pure specimen. The data can be better represented by

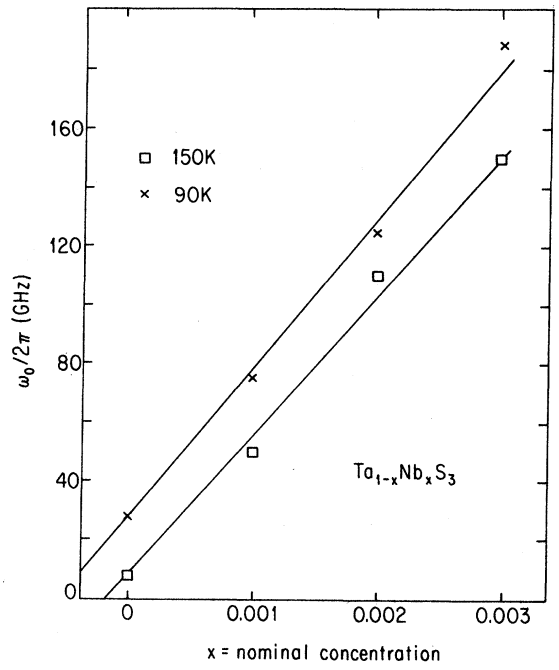

FIG. 16. Concentration dependence of the pinning frequency ω_0 at two different temperatures, $T=150$ and 90 K.

$$\omega_0=\omega_0(\text{pure})+Bx \ , \tag{26}$$

with $B\approx 500$ GHz/at. %. Equation (26) suggests that the parameter B is determined by the choice of impurities, that B is weakly temperature dependent, and ω_0(pure) is of different origin. In the absence of the detailed studies of ω_0(pure) as the function of sample size or preparation conditions, it is impossible to locate the origin of the pinning frequency in the pure specimen. There may, however, be other types of microscopic disorder, such as vacancies or impurities, that do not match the valence of tantalum and contribute a pinning potential with a different temperature dependence. In nominally pure TaS_3, commensurability, grain boundaries, or surfaces may be responsible for the pinning.

Figure 15 shows that, within experimental error, the damping is independent of the impurity concentration, and, to a first approximation, it can be written as

$$\frac{1}{2\pi\tau}=A+BT^n \ , \tag{27}$$

with $n\sim 1$, $A=85$ GHz, $B=0.3$ GHz/K. Because of a weak temperature dependence and large residual resistivity, we cannot exclude a higher exponential n and a weakly-concentration-dependent B. Equation (27), however, is surprising and is unaccounted for at present. First, although the temperature-dependent term can be thought of as caused by the interaction of the collective mode with the uncondensed electrons and/or with the phonons, both mechanisms lead to temperature dependence stronger than that given by the nearly linear dependence found experimentally. We cannot exclude a T^2 temperature dependence on the basis of the experimental data, a finding in agreement with the predictions of Takada *et al.*[31] [Eq. (21)]. As discussed elsewhere, the numerical estimates of B are an order of magnitude smaller than the measured value of B. The large "residual damping" $[2\pi\tau(T=0)]^{-1}$ is also difficult to understand. For damping due to phonons, or normal electrons $1/2\pi\tau(T=0)=0$, the damping goes to zero at zero temperature, and for a damping determined by impurities, $1/2\pi\tau$ should increase with increasing impurity concentration. The highly unusual residual damping, which we found to be independent of the impurity concentration, is unexplained at present and will be discussed in more detail below.

Figures 9–13 clearly show that the fits are qualitative in nature. The actual line shape departs from the harmonic-oscillator fit significantly. As discussed earlier, the deviation is explained at higher temperatures in the nominally pure material by including a distribution of resonant frequencies,

$$P(\omega)=\begin{cases}1/\omega_c, & \omega<\omega_c\\ 0, & \omega>\omega_c \ .\end{cases} \tag{28}$$

The dashed line in Fig. 8 is deduced from such a distribution by convoluting it with a harmonic-oscillator complex conductivity (see Ref. 16),

$$\sigma(\omega)=\int_0^\infty d\omega' P(\omega')\frac{i\omega\sigma_{\max}}{i\omega+\tau[\omega^2-(\omega')^2]} \ . \tag{29}$$

Figure 8(b) displays Im$\sigma(\omega)$ at the same temperature. The positive Imσ below ω_0 and the negative Imσ above ω_0 are again characteristic of a harmonic-oscillator response. Because the fit to Eq. (23b) does not agree in detail at low frequencies [just as with the fit to the real part of the conductivity in Fig. 8(a)], we must use the same distribution to obtain an accurate fit. The fits including a distribution are excellent, as is clear from Fig. 8. Qualitatively, the distribution fit succeeds by broadening the resonance to lower frequencies. In contrast, the deviations from Eq. (1) at lower temperatures or at higher impurity concentrations require a sharpening of the leading edge of the resonance. The model presented in Ref. 5 is therefore clearly inadequate for describing the NB-doped samples.

The impurity-pinning model has been extended[8,9] recently to include intrinsic damping of the CDW response. Using the phase Hamiltonian [Eq. (14)] to derive the impurity-pinning and elastic forces, one can replace the phenomenological pinning term $\omega_0^2\phi$ in Eq. (1), leading to

$$\frac{d^2\phi}{dt^2}+\frac{1}{\tau}\frac{d\phi}{dt}-c_0^2\frac{d^2\phi}{dx^2}-V_0\rho_1\frac{\pi}{m^*\lambda}\sum_i \sin[Qx+\phi(r_i)] =\frac{e}{m^*\lambda}E \ , \tag{30}$$

where c_0 is the phason velocity. The erroneous cosine in Eq. (3) of Ref. 8 has been replaced with a sine. The above expression may be approximately solved with a self-consistent Born approximation,[8] leading to a frequency dependent conductivity

$$\sigma(\omega)=i\omega\frac{ne^2}{m^*}\frac{1}{\omega^2+i\omega/\tau+\Sigma(\omega)} \ , \tag{31}$$

where $\Sigma(\omega)$ satisfies the self-consistent condition

$$\Sigma(\omega)=-\gamma\omega_0^2+\frac{i\omega_0^3}{4[\omega^2+i\omega/\tau+\Sigma(\omega)]^{1/2}} \ , \tag{32}$$

and where γ is a constant of order unity and $\omega_0=n_i\alpha^{2/3}c_0$. The third term in the denominator of Eq. (31) has the role of introducing a frequency-dependent damping that decreases as the frequency is increasing. This term broadens the response at lower frequencies, but remains close to harmonic-oscillator response at higher frequencies, exactly as observed in nominally pure TaS_3 (Ref. 2) (see Fig. 8) and $NbSe_3$.[18] In addition, Im(σ) decreases relative to the harmonic-oscillator value at frequencies below the maximum in Re(σ). A frequency-dependent conductivity with the opposite properties—a broadening of Re(σ) to higher frequencies and an increase of Im(σ) at frequencies below the maximum in Re(σ)—is not possible within this model when $1/\tau>\omega_0$.

The results in Figs. 9–13 are clearly in contrast to this approach. In Fig. 13, for $Ta_{0.998}Nb_{0.002}S_3$, all the experimental results are below the harmonic-oscillator fit [Eq. (23a)] to Re(σ) and above the harmonic-oscillator fit [Eq. (23b)] to Im(σ). Similar effects are observed at higher temperatures (Figs. 11 and 12). The calculations of Ref. 8 are in the weak-pinning limit and imply that ω_0 is proportional to $n_i^{1/3}$. This implication is in disagreement

with Fig. 16 and Eq. (26), where the pinning frequency is linear in the impurity concentration.

Clearly, a theory involving an intrinsic damping and strong rather than weak impurity pinning may be useful in further interpretation of these experimental results.

Bardeen[7] has proposed an alternate approach to describe the dynamics. In this model the frequency-dependent conductivity arises from excitations across a pinning gap. Taken at face value, this model would imply a sharp onset of frequency-dependent conduction, just as observed at lower temperatures on the leading edge of the doped-sample resonance. A functional form for fits in the inertial regime has not been proposed for the tunneling model, so the agreement is only qualitative.

Quantum models would possibly explain an additional feature of the results. The damping of a dynamical response is usually described as arising from impurities or intrinsic excitations of the pure crystal. Here, however, we have a very weak temperature dependence of the linewidth, $1/\tau$ (see Fig. 15), only partially in agreement with the phonon-scattering mode, Eq. (21). Figure 15 shows that the linewidth is also weakly impurity dependent, in clear disagreement with impurity scattering. Another linewidth mechanism, common in semiconductor spectroscopy, is a bandwidth where quantum fluctuations produce a single electron absorption line that is broad at zero temperture in an impurity-free sample. Although a theory of this type is not available, we note that the quantum-fluctuation energy scale for an arbitrary system is given by

$$E=\frac{h^2}{2M\lambda^2}$$

where M is the particle mass and λ is the separation between particles. For metals $M\simeq m_e$ and λ is a few angstroms, leading to $\simeq$5-eV bandwidths. In the CDW case we take $M=2m^*$, the bipolaron mass, and λ to be the CDW wavelength (the bipolaron separation). We evaluate this at $T=150$ K with $m^*=940m_e$, $\lambda=13.4$ Å,[33] and express the result as a frequency, $\nu=E/h=107$ GHz. The close agreement between ν and the experimental value of the linewidth, $(2\pi\tau)^{-1}$, combined with the weak impurity dependence and weak temperature dependence, lead us conclude that quantum concepts may be necessary to describe the dynamics of the CDW.

Finally, we compare the measured pinning frequency with the measured low-frequency dielectric constant and with the measured threshold field E_T. Others have investigated both on specimens from the same preparation batch on which our experiments were conducted. The low-frequency dielectric-constant experiments were conducted at $\omega/2\pi=1$ MHz, a frequency significantly smaller than ω_0. The dielectric constant displays a weak frequency dependence at $\omega\ll\omega_0$, in contrast to the prediction of Eqs. (23a) and (23b), and therefore $\epsilon(1\text{ MHz})$ cannot be regarded as the true $\epsilon(\omega\rightarrow 0)$ limit. Consequently, the arguments based on the low-frequency dielectric constant have only a semiquantitative significance. Figure 17 displays all three parameters, ω_0, $\epsilon(\omega\rightarrow 0)^{-1/2}$, and $E_T^{1/2}$, measured at $T=150$ K as the function of the nominal Nb

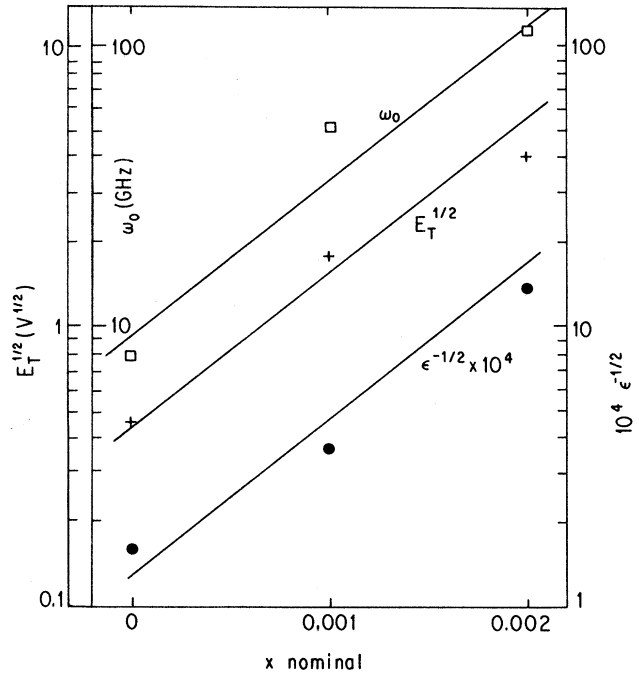

FIG. 17. Concentration dependence of ω_0, $[\epsilon(1\text{ MHz})]^{-1/2}$ and $E_T^{1/2}$ at $T=150$ K.

concentration. Both in the strong pinning limit and in the weak pinning limit [see Eqs. (16) and (17)], both E_T and $\epsilon^{-1}(\omega=0)$ are proportional to ω_0^2, and this is confirmed by the experimental results. The numerical estimates of ϵ and E_T are, however, in clear disagreement with the experimentally found parameters. As α is close to 1, both the weak and strong-impurity-pinning limits give the same order-of magnitude values for ϵ and E_T. For the pure material using $m^*=940m_e$, $n=6.5\times 10^{21}$/cm^3, $\beta=1$, $\lambda=4a_0=12$ Å, and $\omega_0/2\pi\approx 8$ GHz leads to $\epsilon(\omega=0)=9\times 10^6$ and $E_T=20$ V/cm, in contrast to the measured values of $\epsilon(1\text{ MHz})=4\times 10^7$ and $E_T=0.2$ V/cm. The disagreement in the case of $\epsilon(\omega=0)$ is easily explained by the unusual shape of the resonance, where the tail extending to low frequencies adds substantially to the dielectric constant at lower frequencies. In addition, the resonant frequency is not clearly defined for an overdamped resonance, and a value $\omega_0=4$ GHz leads to excellent agreement with $\epsilon(1\text{ MHz})$ without compromising the high-frequency fits.[2]

The difference between the experimental values of E_T and those predicted by Eq. (16) is more substantial. The arguments leading to Eq. (16) assume that a displacement of the CDW by a length $\lambda/4$ is necessary to achieve depinning. That experiment and theory differ by a factor of 100 could imply that the phase displacement necessary to achieve a sliding CDW is of order 1°. This finding is in agreement with nuclear-magnetic-resonance studies[34] of sliding CDW's in $NbSe_3$ that establish that the phase is typically advanced by a few degrees at E_T. An alternate explanation for the discrepancy in E_T is that the non-

linear conduction is associated not with the microwave resonance, but with the spectral weight extending to low frequencies. The effective ω_0 is then much smaller, implying a lower E_T. This possibility is supported by experiments in several materials which show that the limiting nonlinear conductivity is activated[35] and the activation energy is approximately equal to the activation energy of the low-frequency conduction.

The above analysis strongly suggests that the main resonance, which appears in the millimeter-wave spectral range, is not simply related through a single-degree-of-freedom dynamics to the low-frequency and dc properties. The large low-frequency dielectric constant indicates a large low-frequency spectral weight, which also has a strong temperature dependence at low temperatures. Figure 18 shows the temperature dependence of the two parameters. Both $\epsilon(1\ \text{MHz})$ and E_T display a characteristic temperature dependence that has been discussed earlier in the literature. In contrast to the double-peaked ϵ and corresponding $E_T(T)$ that has two minima, ω_0 displays monotonic rise with decreasing temperature. Although we do not understand $\omega_0(T)$ and the increasing pinning forces with decreasing temperature, Fig. 18 obviously shows that ω_0 is not simply related to $\epsilon(1\ \text{MHz})$ and E_T.

V. CONCLUSIONS

We have studied the pinned CDW mode in $(Ta_{1-x}Nb_x)S_3$ alloys in the millimeter-wave spectral range. At high temperatures, $100\ \text{K} < T < T_p$, the response can be approximately described by a harmonic oscillator [Eq. (1)] with a pinning frequency ω_0, effective mass m^*, and damping constant $1/\tau$. A distribution of pinning frequencies, which has been used to describe the experimental results in nominally pure TaS_3, does not appear to be important in the alloys.

In agreement with theoretical expectation, we find that the pinning frequency increases with increasing impurity content, with the frequency increasing approximately linearly with nominal impurity concentration. The temperature and concentration dependence of ω_0 is well described by Eq. (26), which suggests that impurities introduce an additional temperature-independent contribution to the restoring force, with ω_0 in the nominally pure material being strongly temperature dependent. This temperature dependence has not been explained. Arguments advanced by Maki[36] for the behavior of the threshold field may be relevant also for the pinning frequency.

The damping that characterizes the high-frequency ($\omega > \omega_0$) response of the pinned CDW condensate does not, within experimental error, depend on the impurity concentration and appears to be of intristic origin. The scattering of the collective mode from uncondensed electrons, phasons, or phonons depends on the density of the scatters, which should rapidly decrease as the temperature is lowered. The weak temperature dependence of the damping or linewidth must then be explained by more complex models, possibly including quantum effects, which are not yet available.

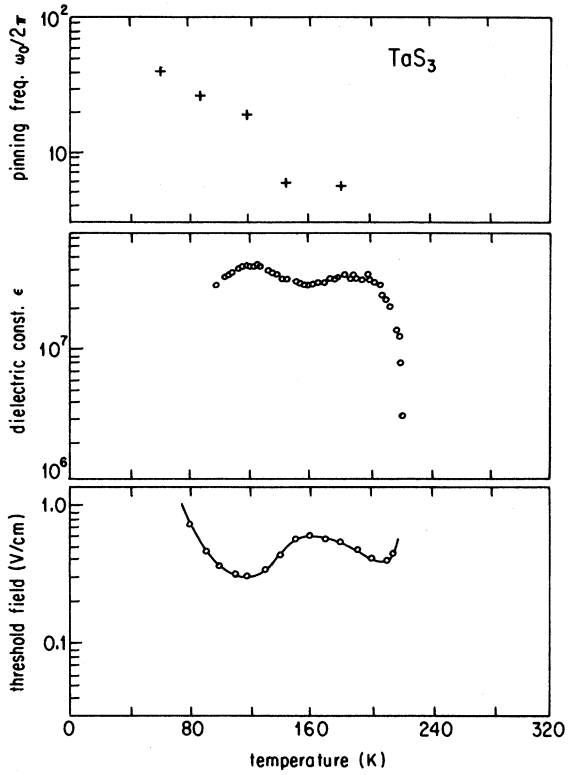

FIG. 18. Temperature dependence of the pinning frequency ω_0, dielectric constant $\epsilon(1\ \text{MHz})$, and threshold field E_T in nominally pure TaS_3.

We have also attempted to relate the pinning frequency ω_0 to the low-frequency ($\omega/2\pi = 1$ MHz) dielectric constant and the threshold field E_T for the onset of nonlinear conduction. Simple arguments, based on the depinning of the collective mode as a rigid entity, lead, however, to $\epsilon(1\ \text{MHz})$, which is orders of magnitude smaller, and to E_T, which is orders of magnitude larger, than the measured values. It is evident from the analysis that the low-frequency, and also low-field, response of CDW's is dramatically different from a single-degree-of-freedom classical dynamics. Others have suggested that tunneling effects[7] or internal distortions[9] with normal electron screening are responsible for the low-frequency behavior of the pinned CDW condensates.

ACKNOWLEDGMENTS

These studies were supported by the National Science Foundation Grant under DMR-86-20340. The authors thank John Bardeen for useful discussions and S. Sridhar, Wei-Yu Wu, A. Janossy, and L. Mihaly for contributing some of the experimental results presented in this paper. One of us, D. R., was supported by the U. S. Department of Energy during preparation of this manuscript.

[1]For a review, see G. Grüner and A. Zettl, Phys. Rep. **119**, 117 (1985), and the articles in *Charge Density Waves in Solids,* Vol. 217 of *Lecture Notes in Physics,* edited by Gy. Hutiray and J. Sólyom (Springer, New York, 1986).

[2]See, for example, S. Sridhar, D. Reagor, and G. Grüner, Phys. Rev. B **34**, 2223 (1986); D. Reagor, S. Sridhar, and G. Grüner, *ibid.* **34**, 2212 (1986).

[3]M. J. Rice and S. Strassler, in *One Dimensional Conductors, Lecture Notes in Physics,* edited by H. J. Schuster (Springer-Verlag, Berlin, 1974).

[4]G. Gruner, A. Zawadowski, and P. M. Chaikin, Phys. Rev. Lett. **46**, 511 (1981).

[5]Wei-Yu Wu, L. Mihály, G. Mozurkewich, and G. Grüner, Phys. Rev. B **33**, 2444 (1986).

[6]R. J. Cava, R. M. Fleming, R. G. Dunn, and E. A. Reitman, Phys. Rev. B **31**, 8325 (1985).

[7]John Bardeen, Physica B+C **143B**, 14 (1986), and references therein.

[8]M. Bleher, Solid State Commun. **63**, 1071 (1987).

[9]P. Littlewood, Phys. Rev. B **36**, 3108 (1987); M. O. Robbins and R. A. Klemm, *ibid.* **34**, 8496 (1986).

[10]J. R. Tucker, W. G. Lyons, and G. Gammie, Phys. Rev. B **38**, 1148 (1988).

[11]D. Reagor, S. Sridhar, M. Maki, and G. Grüner, Phys. Rev. B **32**, 8445 (1985).

[12]A. Philipp, W. Mayr. T. W. Kim, and G. Grüner, Solid State Commun. **62**, 521 (1987).

[13]H. Fukuyama and P. A. Lee Phys. Rev. B **17**, 535 (1987); P. A. Lee and T. M. Rice, *ibid.* **19**, 3970 (1979).

[14]D. Reagor and G. Grüner, Phys. Rev. Lett. **56**, 659 (1986).

[15]P. L. Hsieh, F. deCzito, A. Janossy, and G. Grüner, J. Phys. (Paris) Colloq. **44**, C3-1753 (1983).

[16]S. Sridhar, D. Reagor, and G. Grüner, Phys. Rev. B **34**, 2223 (1986).

[17]Wei-Yu Wu, A. Janossy, and G. Grüner, Solid State Commun. **49**, 1013 (1984).

[18]D. Reagor, S. Sridhar, and G. Grüner, Phys. Rev. B **34**, 2212 (1986).

[19]J. A. Osborn, Phys. Rev. **67**, 351 (1945).

[20]H. A. Bethe and J. Schwinger, National Defense Research Committee Report D1-117, Cornell University, 1943 (unpublished).

[21]L. I. Buravov and I. F. Schegolev, Prib. Tehk. Eksp. Instrum. Exp. Tech. (USSR) **14**, 171 (1971) [Instrum. Exp. Tech. **14**, 528 (1971)].

[22]S. Sridhar, D. Reagor, and G. Gruner, Rev. Sci. Instrum. **56**, 1946 (1985).

[23]J. Schwinger, and D. Saxon, *Discontinuities in Waveguides* (Gordon and Breach, New York, 1968).

[24]H. Mutka, S. Bouffard, G. Mihály, and L. Mihály, J. Phys. (Paris) Lett. **45**, L-113 (1984).

[25]See, for example, P. Monceau, in *Electronic Properties of Inorganic Quasi-One-Dimensional Compounds,* edited by P. Monceau (Reidel, Dordrecht, 1985), Pt. 2, p. 139.

[26]H. Fukuyama, J. Phys. Soc. Jpn. **45**, 1474 (1978); **41**, 513 (1976).

[27]K. B. Efetov and A. I. Larkin, Zh. Eksp. Teor. Fiz. **72**, 2350 (1977) [Sov. Phys.—JETP **45**, 1236 (1977)].

[28]L. Mihály and G. Grüner, in *Nonlinearity in Condensed Matter,* Vol. 69 of *Springer Series in Solid State Sciences,* edited by A. R. Bishop (Springer-Verlag, Berlin, 1987).

[29]L. J. Sham and B. R. Patton, Phys. Rev. B **13**, 3151 (1976).

[30]Y. Imry and S.-k. Ma, Phys. Rev. Lett. **35**, 1399 (1975).

[31]S. Takada, M. Wong, and T. Holstein, in *Charge Density Waves in Solids,* Vol. 217 of *Lecture Notes in Physics,* edited by Gy. Hutiray and J. Sólyom (Springer-Verlag, Berlin, 1985), p. 227.

[32]P. A. Lee, T. M. Rice, and P. W. Anderson, Solid State Commun. **14**, 703 (1974).

[33]H. Salva, Z. Z. Wang, P. Monceau, J. Richard, and M. Renard, Philos. Mag. B **49**, 385 (1984).

[34]J. Ross, Z. Wang, and C. P. Slichter, Phys. Rev. Lett. **56**, 663 (1986).

[35]R. M. Fleming, R. J. Cava, L. F. Schneemeyer, E. A. Rietman, and R. G. Dunn, Phys. Rev. B **33**, 5450 (1986).

[36]K. Maki, Phys. Rev. B **33**, 2852 (1986).